RESEARCH PAPER

A Hybrid Deep Feature Aggregation and Adaptive Weighted Classifier Model for Robust Cytogenetic Screening of Down Syndrome

B.L.Shivakumar[1], U.Priya [2]

1Principal, Department of Computer Science,Sri Ramakrishna College of Arts and Science, Coimbatore-641 006
Email : blshiva@gmail.com
2Research Scholar,Department of Computer Science, Sri Ramakrishna College of Arts and Science,Coimbatore-641 006
Email :priyatamilelango@gmail.com

ABSTRACT
The systematic genome analysis platform is presented to increase the automation and accuracy of chromosome-based detection in Down syndrome. This research aimed to overcome the significant problems in cytogenetic image processing, such as noise interference, boundary ambiguity and structural integrity loss during processing. The main goal is to create an end-to-end system that achieves high-fidelity denoising, sharp segmentation, more content feature extraction and strong classification. The proposed methodology combines four main modules, namely Entropy-Guided Denoise Network (EGD-Net) usedfor entropy-guided noise reduction,Genomic Structure Fragmenting Network (GSF-Net) usedfor multi-stage genomic segmentation, Hybrid Transform Feature Aggregator (HTF-A) used for Feature Extraction and Adaptive Weighted Pattern Recognition (AWPR-Net)used for Classification. The image of the chromosomes is gradually narrowed in each module and the key patterns of the genome are maintained. TheResults illustrate significant improvements whencompared tocurrent methods. The EGD-Net proposed a PSNR of 41.27 dB and SSIM of 0.981, which validates the use of the method in noise reduction and preserving structure. The general classification phase reached an accuracyof 94.741% which has good reliability in differentiating normal and abnormal chromosomes. These measures prove that the suggested multi-stage design is solid.The conclusion proves that the integrated pipeline provides higher visual quality, better structural mapping and more powerful predictability. The framework applies a realistic resolution to genomic screening settings, which are based on robust, dependable and high-resolution interpretation of chromosomes
Keywords: : Chromosome Segmentation, Down Syndrome Detection, Feature Aggregation, Genomic Image Analysis, Pattern Classification, Prenatal Screening.
How to cite this article: Shivakumar BL, Priya U, A Hybrid Deep Feature Aggregation and Adaptive Weighted Classifier Model for Robust Cytogenetic Screening of Down Syndrome .Int J Drug Deliv Technol. 2026;16(2s): 247-265; DOI: 10.25258/ijddt.16. 247-265
Source of support: Nil.
Conflict of interest: None

INTRODUCTION

Down syndrome is a genetic disorder that is precipitated by the extra chromosome 21 which provides physical, cognitive, and developmental problems that require early and proper diagnosis. Conventional clinical screening relies on ultrasound measurement, serum biomarker and manual chromosomal analysis which has been criticized to be operator-dependent and subjective. Recent advances in the sphere of artificial intelligence have improved automated detection of Down syndrome, in particular, by the use of the face image with deep learning applications and the prenatal picture [1]. Fetal level prediction systems are also developed and have assisted in risk assessment at an earlier stage with there is application of clinical and demographic factors [2]. In addition,has improved accuracy, especially in the most recent ultrasound-based diagnostic treatments which entail integration of both computational and automated measure processes in the screening procedures [6]. Even after such improvements, one can still note challenges that are linked to noise distortions, uneven light distribution, and minute structural variations which reduce the reliability of diagnostics. In order to classify correctly, there is also the need to preserve the delicate genomic patterns more by ensuring that automated segmentation and extraction of the features is achieved. These limitations highlight the need to have an end-to-end, automated diagnostic system that is high-fidelity. This research, consequently, provides an entire genomic analysis workflow to support plausible and prompt diagnosis of Down syndrome.

Several AI-implicated researchstudies have also contributed to the initial risk prediction with the addition of multimodal features and hybrid learning systems to the first-trimester screening, and offer a significant addition to the diagnostic sensitivity [3]. The processes made out of the facial metric have also contributed to the verifiable gains of initial childhood Down syndrome recognitionwith discriminative geometrical patterns [4]. Deepest forms of recognition improved the level of phenotypic differentiation and increased the level of accuracy that patterns were detected [5]. To optimize automated early screening with precision-enhanced imaging pipelines [6], and poorer homologous anatomic facial-metric models were suggested to be more reliable in phenotype recognition tasks [7], new fetal ultrasound-based methods were underway. The image classification frameworks that relied on CNN-driven

**Author for Correspondence: Prof. Dr. Cuneyt Karaarslan MD*

approaches found control through the use of phenotypes were demonstrated to possess an effective capacitywith Down syndrome and Williams syndrome [8]. As well, there were assistive systems to help people with Down syndrome and integrate object recognition into the assistive tools in real time [9]. Additionally, the serum-screening processes at the scale of big populations have been simplified by the qualitymonitoringwith the help of AI [10]. These gaps and strengths of the literature have led the proposed research to propose an integrated framework that consists of EGD-Net to perform denoising, GSF-Net to perform segmentation, HTF-A to perform feature aggregation, and AWPR-Net to perform adaptive classification to build a robust, accurate and structurally preserved Down syndrome detection pipeline.

The article presents a full-fledged pipeline of multiple multiphase chromosomes consisting of denoising, segmentation, feature mining, and classification. The entropy approach to denoising methodology conserves potential sensitive genomic structures compared to the conventional approaches. Transfer-based feature aggregator improves the multi-scale chromosome representation and structural learning. Both normal and abnormal genomic pattern differences are boosted using an adaptive weighted classifier. Integrated architecture has never been at the state of art in terms of precision, resilience and sustenance of structural integrity.

Organization: Section 1 introduces the concept of chromosome-based detection of Down syndrome, the motivation, clinical value, and literature as the justification. Section 2 is the background researchwherean overview of the already existing research findings and the limitationsthat should be ameliorated by means are identified. This suggested methodology is presented in the third section and includes EGD-Net, GSF-Net, HTF-A, and AWPR-Net as one genomic analysis pipeline. Section 4 addresses the experimental evaluation in which the visual outputs, comparative measures, and validation of the performance at each processing step are provided. Section 5 gives the conclusion and demonstrates the overall success, influence, and diagnostic merit of the combined design of the chromosome examinations.

2. LITERATURE REVIEW

Reshi et al. (2024) [11] paid attention to the early assessment of Down syndrome with the help of fetal ultrasound images. used a deep learning-based architecturethat used (Nuchal Translucency) NT and anatomical features to improve the accuracy of classification. The gap of inconsistencies in the interpretation of the manuals and inadequate automated diagnostic tools was also a topic of the research. Their findings showed that they were better predictors than the conventional ultrasound analysis.

Sonia and Shanthi (2016) [12] studied the issue of early diagnosis of Down syndrome through assessment of the nuchal translucency thickness of the fetus using ultrasound images of the first trimester. used image-processing methods to localize the NT area and compute the thickness accurately. bridged the gap of manual NT measurement error and manualism. The results indicated that the computer-aided measurement of NT enhanced the reliability of the screening of DS.

The research by Gonzalez-Gonzalez et al. (2019) [13] involved the development of computational thinking in children with Down syndrome using the KIBO robotused interactive skills that were based on robotics learning to aid in cognitive skill development. The research was aimed at the shortage of technological applications that could be used by the DS students. Their research indicated that there wasa positive interaction and better performance in learning by the involved children.

The article by Thomas and Arjunan (2022) [14] suggested a deep learning-based measurement of the nuchal translucency region to assist in early diagnosis of Down syndrome. used CNN-based segmentation to enhance accuracy in extracting NT boundaries. Their work aimed to fill in holes in precision due to manual and semi-automated methods of NT measurement. The model generated very precise NT segmentation findings and minimized the variability in the diagnosis.

A probabilistic neural network classifier was designed by Rahmat et al. (2020) [15] to identify children with Down syndrome based on their faces. First of all, extracted face features and trained a PNN(Probabilistic Neural Network)model to classify DS and non-DS faces. The research dealt with the lack of simple and low-complexity classification models of DS detection. found that PNN was reliable with minimum training data.

Research by Mariselvam et al. (2023) [16] developed an AI-driven virtual reality play therapy system on wheelchair-bound children with Down syndrome. combined reinforcement learning to modify therapy actions depending on user behavior. The research bridged the research gap on individualized, easily accessible rehabilitation interventions forchildren with DSmobility difficulties. Their findings showed that they interacted better, were more engaged and responsive to therapy.

Robles-Bello et al. (2020) [17] investigated variables that could forecast the success of early reading interventions with children with Down syndrome. To determine important variables, used the use of psychological tests and statistical models. The research dealt with a lack of knowledge on personal predictors that influence the development of DS learning. Their results emphasized that there were major cognitive and behavioral indicators related to improved intervention outcomes.

The frequency of mosaic Down syndrome and comorbid medical issues was the focus of an analysis conducted by Rubenstein et al. (2024) [18] among adults with Medicaid enrollment. The assessed health record information to describe clinical trends and comorbidities. The research addressed the paucity of large-scale research about the population of adult mosaic DS. Their findings revealed mixed prevalence of related conditions, which can be used in healthcare planning.

The article by Hunter et al. (2023) [19] examined the issue of transcription dosage compensation in people with Down syndrome. performed both genomic and transcriptomic research to investigate the balancing of the expression. The research was concerned with the gap in knowledge of whether the trisomy of chromosome 21 initiated compensatory regulation of genes. Their findings validated the fact that transcription dosage compensation was not found in DS, and gave new insight into the genetic expression theories.

A Multiscale Quantiser, along with a convolutional neural network was developed by Simon and Kavha (2021) [20] to create a method of detecting Down syndrome through ultrasound. Multiscale feature extraction was used and then deep learning classification was used. The research dealt with the necessity to have automated and precise ultrasound-based DS detection structures. Their system had high detection and feature representation.

In the article by Zamm et al. (2020) [21], the authors examined the amyloid accumulation in subjects with Down syndrome by means of amyloid-load imaging. used the PET scans and quantitative imaging biomarkers to determine the patterns of cerebral amyloid. The research provided missing information on early AD risk evaluation in DS groups. Their findings proved high amyloid deposition thus proving that DS is a high-risk group regarding dementia.

In e-health record data, Baksh et al. (2023) [22] researched several morbidities throughout the lifespan of people with Down syndrome. conducted longitudinal analysis to define the prevalence and disease progressions authors examined low population-level data on the long-term health in individuals with DS. Their findings showed that had different multimorbid patterns as compared to normal populations.

Krivonosov et al. (2020) [23] investigated the changes in DNA methylation with age in Down syndrome using a paracrine networkcompared DS patients and healthy controls to analyze epigenetic deviations. The research bridged the gap in the modelling of the complex methylation dysregulation during aging in the presence of DS. It found that there were distinct methylation network architectures that involved accelerated aging phenotypes.

Colak et al. (2025) [24] spent their attention on the regions of metabolomics-based biomarker discovery of Down syndrome with the help of a kernel-tree model which is a model of explainable artificial intelligence subjected metabolomics data sets to the discovery of discriminative biomarkers. The research covered the gaps in interpretable AI techniques to use in the context of DS metabolomic profiling. Their findings generated useful biomarkers and provided a high level of transparency in AI decision-making.

3. RESEARCH METHODOLOGY

The proposed methodology proposes a complete genomic pipeline of analysis which begins with a collection of curated chromosome images and which is successively followed by a multi-phase analysis pipeline. The overall structure integrates the denoising, segmentation, feature extraction and classification in order to ensure proper preservation and interpretation of chromosome structures. The reason is that a particular architecture is developed in each of the modules with particular architectural flow, mathematical equations, and optimized calculation principles, which guarantee the ideal genomic refinement. The functional changes in each of the stages are presented in detailed equations, and operational logic is presented and demonstrated with the assistance of pseudocode. methodical arrangement that ensures that there is a similar treatment of raw chromosome specimens up to the last diagnosis category.

3.1 Dataset

https://www.kaggle.com/datasets/aliabedimadiseh/chromosome-image-dataset-karyotype

Aliabedimadiseh chromosome karyotype images dataset is taken from the publicly available Kaggle Website. This dataset contains a set of chromosomes karyogram images in single or multiple chromosomes that can be used in cytogenetic analysis, such as the detection of structural abnormalities.It is made up of normal and abnormal chromosomes therefore,it is suitable in training and testing image classifiers. Theseimages are grayscale karyotype images, that indicate morphologies of clinical cytogenetics. Thisdataset is used for research tasks that include the classification, segmentation and detection of the anomaly of the chromosomes based on diseases.

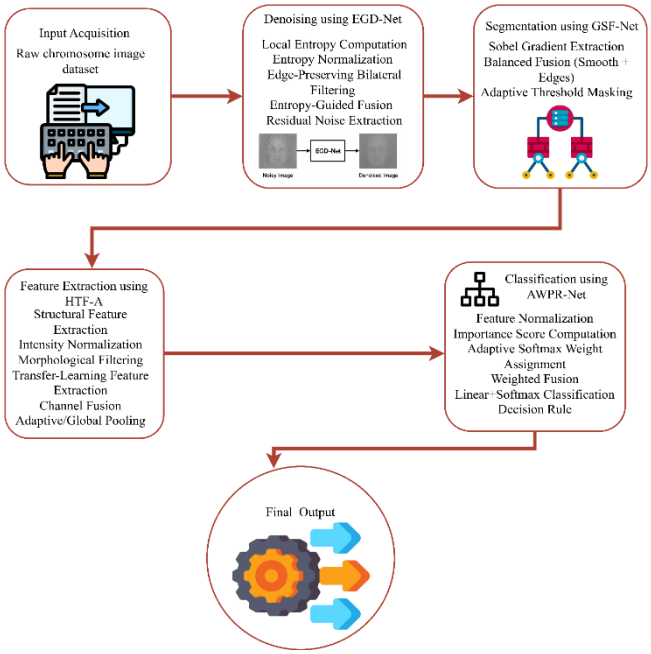

Figure 1: Overall Architecture of the Multi-Phase Chromosome Prediction Framework

In Figure 1, the overall architecture operates as a sequential genomic analysis pipeline that begins with chromosome image input and applies EGD-Net to remove noise while preserving fine chromosomal details. The denoised output is passed to GSF-Net, which enhances structural boundaries and generates a clean segmentation map for isolating each chromosome region. HTF-A then extracts multi-scale structural, intensity, morphological, and transfer-learned

features to create a highly discriminative representation. These fused features are processed by AWPR-Net, which adaptively weights each feature channel for robust classification. The final stage outputs accurate predictions of normal or abnormal chromosomes, completing a fully automated end-to-end diagnostic framework.

3.2 Denoising using the Proposed AlgorithmEGD-Net

The Entropy-Guided Denoise Network proposes an entropic-based dynamically evolving filtering approach, which attempts to improve the quality of genomic images pixel-by-pixel. The algorithm compares the differentials of the local entropy in a per-chromosome basis, and determines structurally important domains, and is discriminative in degrading noise without altering biologically significant motifs. With this step of genomic analysis, EGD-Net enhances the comparisons of the chromosomal extremities, fine-textured structures as well as the preservation of the intrinsic genomic morphology that facilitates a clean and reliable foundation of the subsequent segmentation and detection of abnormal processes.

The traditional methods of denoising have the highest chances of blurring fine textures in genomic sequences, which are susceptible to asymmetric lighting fields, and failing to separate the shallow structural information and noise. The following problems are being addressed by EGD-Net using the entropy-adaptive learning, in which the noise-suppressing dynamic regulator dynamically adjusts the intensity of noise suppression based on the richness of the local information and eradicates the suppression of weak but important chromosomal markers. The intended retention of the genomic information, as well as the strong artifact removal, allows the high-fidelity denoising to be used in diagnostics, resulting in clean and high-quality visual images, even in problematic imaging conditions.

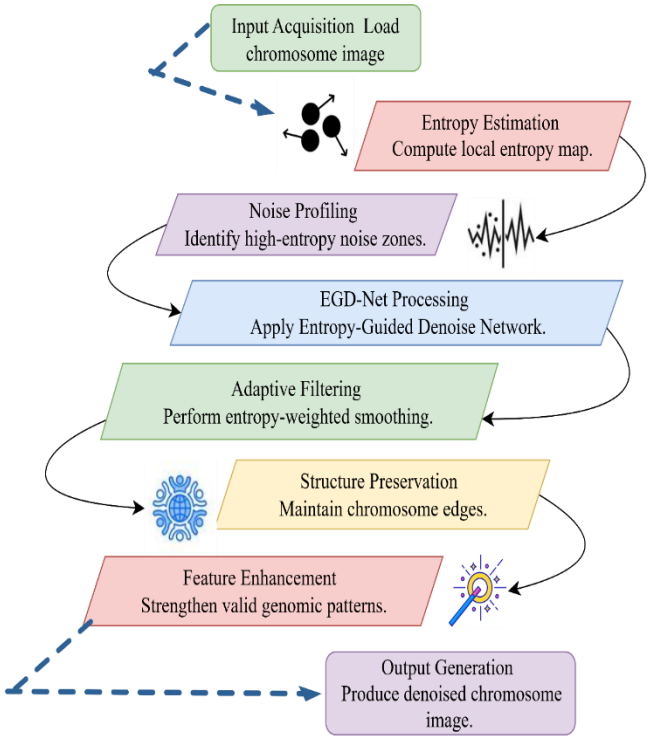

Figure 2: EGD-Net DenoisingArchitecture

InFigure 2, EGD-Net uses local entropy map to locate high information regions of the chromosomes and retrieves the high information regions and eliminates low-entropy noise. bilaterally filters to retain the edge structures and averages by averaging using entropy adaptive weights the original image and the smoothed image. The network can improve the appearance of contrast and banding without need of extra cost in fine chromosomal textures. The last residual map isolates the noise, which would create structural fidelity. The architecture is used to provide a high-quality and clean image to downstream segmentation.

$(x,y) - - \sum_{k=1}^{K} p_k(x,y) log_2 \left(p_k(x,y)\right)$ ----------(1)

In Equation (1) $E(x,y)$ local entropy of pixel (x,y),$p_k(x,y)$ normalized histogram probabily of the gray-level bin k in the local neighborhood around (x,y),$k$number of histogram bins used in the local window depending on the size of the local neighbourhood.Local entropy is used to measure the variation of the intensity at pixel(x,y) high E means rich texture and structure, and low E means uniform background. computes a local histogram and uses Shannon entropy to highlight sections of the information that contain high information content in the data.

$\tilde{E}(x,y) = \frac{E(x,y)-min(E)}{max(E)-min(E)+\varepsilon}$----------(2)

In Equation (2) $\tilde{E}(x,y)$Value of entropy scaled to [0,1] at pixel (x,y),$min(E)$, $max(E)$global minimum and maximum entropy value,insert small constant,e.g, 10^{-8}) to avoid division by 0.Normalization to always put the value

of the entropy in the [0,1] range, so as to make a stable per-pixel weighting maskvalues near 1 indicate detailed regions, values near 0 indicate flat/background regions.

$B(x,y) = B(I;\sigma_c,\sigma_s)(x,y)$ ----------(3)

In Equation(3) $B(x,y)$Lateral-filtered intensity at$I(x,y)$original normalized grayscale intensityat$B(I;\sigma_c,\sigma_s)$ bilateral filter operator withintensity sigma σ_c and s, σ_s.$\sigma_c$sensitive to change of intensityedge preservation,$\sigma_s$is sensive to change of spatial resolution.The bilateral filter smooths noise, combines spatial proximity and intensitysimilarity and strong edges remain strong and form a clean and structure-conscious image B .

$D(x,y) = \tilde{E}(x,y)I(x,y) + \left(1 - \tilde{E}(x,y)\right)B(x,y)$----------(4)

In Equation (4) the bilateral-filtered intensity $B(x,y)$ and the original normalized intensity$I(x,y)$are used $D(x,y)$Final denoised output at pixel (x,y),$\tilde{E}(x,y)$ normalized entropy weight (0–1),I(x,y)original normalized intensity.

$R(x,y) = I(x,y) - D(x,y)$ ----------(5)

$R(x,y)$residual at (x,y),$I(x,y)$ original intensity, $D(x,y)$denoised fused intensity in Equation (5) The values within the residual show that the denoising operation has removed and is useful in determining quality or in further optimization.

Algorithm 1: Entropy-Guided Denoise Network (EGD-Net)

Input:

I ← Input chromosome grayscale image (normalized to 0–1)

w ← Window size for local entropy computation

σ_c← Range sigma for bilateral filter

σ_s ← Spatial sigma for bilateral filter

ε ← Small constant for numerical stability

Begin

1. Compute Local Entropy Map:

For each pixel (x, y) in I:

Nxy ← Local neighborhood window of size w around pixel (x,y)

H ← Histogram of intensities inside N x,y

pk ← Normalize H to obtain probabilities for each bin k

E(x,y) ← - Σ [pk * log2(k)] // Shannon entropy

2. Normalize the Entropy Map:

Emin ← Minimum value in E

Emax ← Maximum value in E

For each pixel (x,y):

$\tilde{E}(x,y) = (\max(E) - \min(E) + \varepsilon$

3. Apply Edge-Preserving Bilateral Filter:

B ← BilateralFilter(I, σ_c, σ_s)

// Produces a smooth image while keeping edges sharp

4. Entropy-Guided Fusion:

For each pixel (x,y):

$D(x,y) = \tilde{E}(x,y)I(x,y) + \left(1 - \tilde{E}(x,y)\right)B(x,y)$

// High entropy → keep original

// Low entropy → use smoothed pixel

5. Compute Residual Map:

For each pixel $I(x,y)$:

$R(x,y) = I(x,y) - D(x,y)$

Return:

D // Final denoised output

R // Residual showing removed noise

Output:

D ← Final denoised chromosome image

R ← Residual (removed noise map)

End

In Algorithm 1 starts with the pseudocode that identifies a local entropy map that identifies the textured and detail-rich segments of the chromosomes. Such an entropy map is scaled and turned into a pixel-wise weight to determine where the details should be retained. A bilateral filter is used to obtain a smoothing and edge-avoiding rendition of the image that is subsequently added to the original after weighting the two images with entropy. Lastly, the map of residual shows the noises that are removed during the denoising process so that it is not obscured when structural genomic information is considered.

3.3 Segmentation using Genomic Structure Fragmenting Network

Genomic Structure Fragmenting Network is a multi-level adapting fragmentation plan, which is to fragment the structures of the chromosomes most finely. Using the refined, denoised image, the algorithm will smooth more and more of the chromosome and remove the noise patterns that have been left behind and strengthen the structural edges that are supported by an edge. GSF-Net detects discrete genomic segments which are well-defined over a combination of a Gaussian smoothing, noise-difference mapping and gradient-based markers of an edge. This classification allows a further contrast to the profile of the chromosomes and the most detailed structure view and a good background on whichdownstream processes of detecting abnormalitiesutilize executed.

The traditional forms of segmentation have been rendered to be baffling with dark edges, overlaps and inconsistent findings in case of inefficient light lighting. To overcome these shortcomings, GSF-Net may take advantage of selective feature increment coupled withnoise-sensitive structural refinement with noise-reliable, in this sense each branch of genetics is specific further subdivided even in the most challenging imaging circumstances. The vibrant combination of the mean patterns of the intensities and the edge values throughout the algorithm obstructs the elimination of the finer details of the chromosomes without being disturbed by the insignificant backgrounds. It is a superb system of segmentation that offers excellent quality and stable structural segregation of the system that could be used in the real time genetic cytogenetic process that can bring a higher quality of accuracy in the segregation and identification of genetic areas and anomalies.

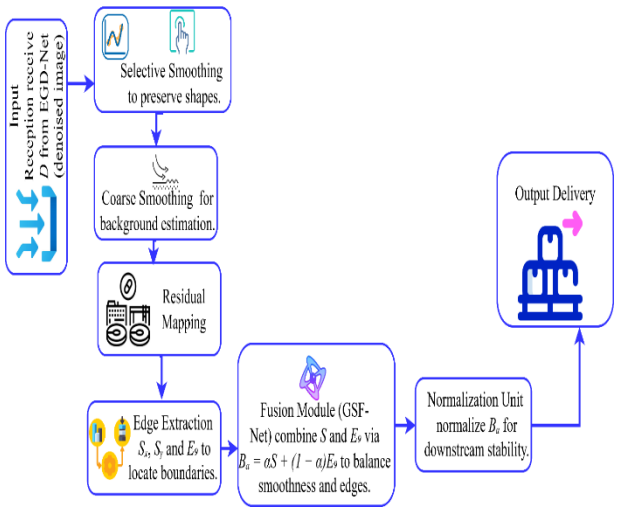

Figure 3: Segmentation Architecture using Genomic Structure Fragmenting Network

Figure 3, the output of the denoised image is fed into GSF-Net as a limitednumber of Gaussian filters to be applied to make the image pixels selectively smoothto further highlight the shape of the chromosomes. computes noise-cutting disparity, Sobel-refined edges and combines these cues and equalizes the enhancement image. Normalization provides an equal intensity mask and adaptive thresholding provides a pure binary segmentation mask. The structure design is made to conserve deliming and also minimize light artifacts and enhance structural clary. This will be to ensure that the chromosomes are extracted to enable extraction of the features.

$$S(x,y) = G_{\sigma 1}\big(D(x,y)\big)\text{----------(6)}$$

In Equation (6) $S(x,y)$was biased to enhance the intensity at the pixel (x,y)after light smoothing, $G_{\sigma 1}(.)$. Gaussian filter operator of $\sigma 1$ (responsive to the scale of smoothing), (e.g., 1.2) to prevent the very small noise and leave the larger-scale shapes of the chromosomes intact, constituting a consistent base of segmentation, $D(x,y)$denoised input intensity at (x,y)(output of EGD-Net, range 01).

$$N(x,y) = D(x,y) - G_{\sigma 2}\big(D(x,y)\big)\text{----------(7)}$$

In Equation (7) $N(x,y)$noise- suppressing (difference) (x,y)image intensity of high-frequency content, $G_{\sigma 2}$ $(\cdot)$Gaussian filter of large sigma σ2 (e.g 3) coarse smoothing, σ2 large Gaussian(x,y).

$$E_g(x,y) = \sqrt{(S_x(x,y))^2 + (S_y(x,y))^2}\text{----------(8)}$$

In Equation (8) $E_g(x,y)$edge strength (structural strength) at the pixel (x,y),$S_x(x,y)$horizontal and vertical Sobel gradient responses calculated using $(D.S_x(\cdot).D(x,y)$denoised input intensity on which the edges are detected. Gradient strength is used to highlight edges and other smaller details of the structure in which the strength has been abruptly changed to reveal the objects.

$$B_a(x,y) = \alpha S(x,y) + (1-\alpha)E_g(x,y)\text{----------(9)}$$

In Equation (9) $B_a(x,y)$ balanced enhancement map (segmentation input) at (x,y)fusion weight (e.g., 0.6) to control the smoothness-edge trade-off. $S(x,y)$ selectively enhanced (smoothed) intensity,$E_g(x,y)$ edge magnitude capturing boundaries.Fusion maintains S to maintain smoothness all over the world, and E_g to maintain sharpness of the edges forming a perfect segmentation map.

$$M(x,y) = \begin{cases} 1, & B_a(x,y) \geq \tau \\ 0, & \text{otherwise} \end{cases}\text{----------(10)}$$

In Equation (10) $M(x,y)$binary segmentation mask(1 = chromosome region, 0 = background),$B_a(x,y)$balanced enhancement value at (x,y), τsegmentation threshold global and adaptive), determining the sensitivity.

Algorithm 2: Genomic Structure Fragmenting Network

Input:
D ← Denoised grayscale image (normalized 0–1) // Denoising output from EGD-Net
σ1 ← Gaussian sigma for selective enhancement (e.g., 1.2)
σ2 ← Gaussian sigma for stronger smoothing (e.g., 3.0)
α ← Fusion weight (0 ≤ α ≤ 1) (e.g., 0.6)
τ ← Optional threshold for mask (optional; if None, use adaptive threshold)
ε ← Small stabilizer (e.g., 1e-8)
Begin
1. // Selective enhancement (mild smoothing)
S ← GaussianFilter(D, sigma=σ1)
2. // Noise suppression map (difference-of-smoothing)
G2 ← GaussianFilter(D, sigma=σ2)
N ← D - G2
3. // Structural edges (gradient magnitude)
S_x** ← SobelFilter(D, axis='x')
S_y← SobelFilter(D, axis='y')
Eg ← sqrt(S_x**2 + S_y**2)
4. // Balanced fusion between smooth and edges
Ba ← α * S + (1 - α) * Eg
5. // Optional: Normalize balanced map for consistent range
$B_a$min, $B_a$max ← min(Ba), max(Ba)
Ba ← (Ba - $B_a$min) / ($B_a$max - $B_a$min + ε)
6. // Optional: Create segmentation mask
If τ is None:
τ ← AdaptiveThreshold(Ba) // e.g., Otsu or local threshold
M ← (Ba >= τ).Astype(uint8)
Return:
S, N, Eg, Ba, M
Output:
S ← Selectively enhanced image (from light Gaussian)
N ← Noise-suppression (difference) map
Eg ← Edge magnitude map (Sobel)
Ba ← Balanced enhancement map (fusion)
M ← Segmentation mask (binary)
End

In Algorithm 2, smoothing of the denoised output D of EGD-Net is then followed to obtain the clean structural baseline S and further smoothing is performed on the output to obtain the difference map of the output N and the difference map of the noise suppression difference map N. This is followed by Sobel operator to obtain structural gradients in order to identify chromosome and fine morphological edge boundaries. The smoothness of S is combined with sharpness of to create the composed enhancement map in a weighted averaging and normalized

to ensure that, there is a fixed scale of intensity variation. This is preceded by a fixed or adaptive threshold to convert to a binary segmentation mask to isolate single chromosome sequences to an exact extent.

3.4 Hybrid Transfer Feature Aggregator for Feature Extraction

The Hybrid Transfer Feature Aggregator is a multi-branch extractor, andis trained on hybrid convolutional mappings and produces multi-scale structural, intensity, and morphological descriptors of the areas of the segmentation of chromosomes. The output of the balanced segmentation is fed as input in the module computing the gradient-based structural maps, intensity normalization, and morphology-conscious transform and assembles all such channels into a small representation whichutilize further fed into down-stream anomaly classifiers. The reason behind the HTF-A is to get the local texture and global shape information at the expense of local chromosomal abnormalitywhich is bound to play a vital role in detecting trisomy.

The conventional feature extractors are commonly ineffective to the multi-scale patterns to be able to operate in different forms of light and to use the already recognized semantic information. These gaps are bridged in HTF-A that uses transfer-learned feature priors, like lightweight hybrid convolutions and explicit morphological operators, that has the ability to transfer potent features across datasets and illumination settings. is composed structured having good structural fineness but with an increase of an invariant value of intensity that forms consistent and reliable features in the case of a real-time cytogenetic protocol and better features are utilized in determining an abnormality in a real-world situation.

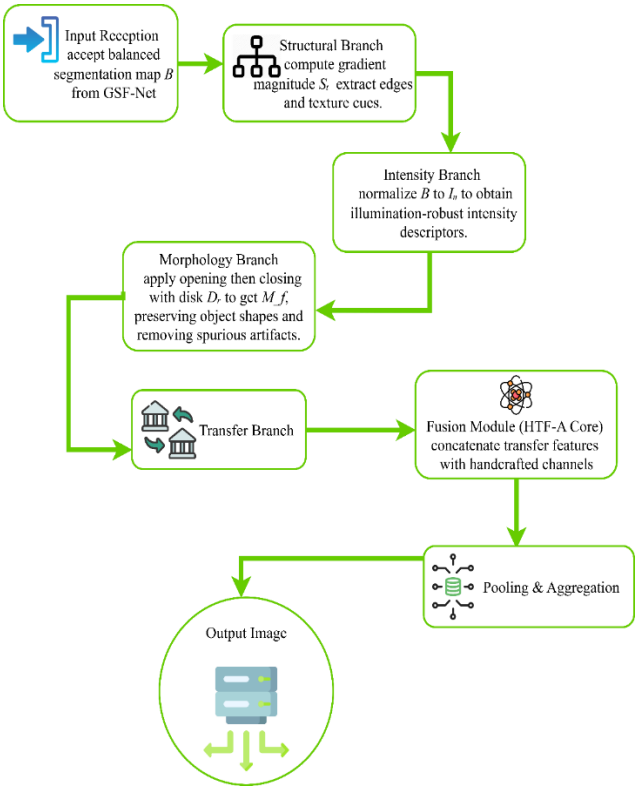

Figure 4: Feature Extraction ArchitectureHybrid Transfer Feature Aggregator

In Figure 4,the HTF-A is applied within the structure of feature extraction to extract the multi-scale chromosome features owing to the integration of structural, intensity, morphological, and pre-trained transfer-learning features. The projection of the division lines is done with the help of a gradient-based map and presentation of illumination-invariant representation is done with the help of the normalization of the intensity. The morphology filtering makes the lines of the shapes sharper and the distortions are removed in order to preserve the geometry of the chromosomes. The learned backbone erases the rich semantic information that can provide a background of meaning. All the feature channels are then combined into a very small vector which offers a very discriminative representation of the actual classification of the chromosomalabnormalities.

To compute the edges and textures, a Structural magnitude gradient is used to compute the gradient.

$S_t(x,y) = (Sobel_x(B(x,y)))^2$----------(11)

In Equation(11), $S_t(x,y)$Strength of structure (edge) in a pixel (x,y),$Sobel_x(\cdot)$horizontal and vertical Sobel gradient derivatives (being similar to tensile gradients) in a pixel (x,y) $B(x,y)$balanced segmentation map input (generated by GSF-Net) in a pixel (x,y).

Normalize the intensity to some fixed 0 to 1 value to get illumination resistant descriptors.

$I_n(x,y) = \frac{B(x,y)-min(B)}{max(B)-min(B)+\varepsilon}$ ----------(12)

In Equation (12)$I_n(x,y)$Normalizedintensity of pixel$(x,y)min(B)$, $max(B)$:global minimum of the balanced map B,εglobal maximum of the balanced map small constant to avoid division by zero, $B(x,y)$balanced segmentation map input.

Reducing artifacts like noise or shape, the morphological context lessens both with opening and closing operations.

$M_f(x,y) = Closing(Opening(B(x,y),D_r),D_r)$--------(13)

In Equation(13),the morphology-filtered image $M_f(x,y)$of the original picture, and morphological (x,y),$Opening(\cdot,D_r)Closing(\cdot,D_r)$and disk-shaped structuring element D_r(radius $rB(x,y)$.

$F = \text{Pool}\left(\text{Concat}(\emptyset_{\text{pre}}(B), S_t, I_n, M_f)\right)$--------(14)

In Equation(14) F final aggregated feature vector (input to classifier), $\emptyset_{pre}(B)$ backbone feature map of pretrained and fixed length, B,$Concat(\cdot)$: channel-wise concatenation operator, $Pool(\cdot)$ spatial pooling (global average or adaptive) that create fixed-length vectors,S_t, I_n, M_f structural, normalized intensity, and morphological maps, which are defined above.

Algorithm 3: HTF-A Feature Extraction (Hybrid Transfer Feature Aggregator)

Input:

B ← Balanced segmentation map (grayscale, normalized 0–1) // Output from GSF-Net

backbone ← Pretrained feature extractor (e.g., ResNet block) // transfer module

r ← Structuring element radius for morphological ops (e.g., 3)
pooltype ← Pooling method ("globalavg", "adaptive")
ε ← Small stabilizer (1e-8)
Begin
1. // Structural map: gradient magnitude
S_x ← Sobel(B, axis='x')
S_y ← Sobel(B, axis='y')
S_{map}← sqrt(S_x**2 + S_y**2)
2. // Intensity normalization
B_{min}← min(B); B_{max}← max(B)
I_{map}← (B - B_{min}) / (B_{max} - B_{min}+ ε)
3. // Morphological filtering (opening then closing)
SE ← Disk(radius=r)
temp ← Opening(B, SE)
M_{map}← Closing(temp, SE)
4. // Transfer feature extraction (hybrid deep features)
Tfeatmap ← backbone.extractfeatures(B) // retains spatial map
5. // Channel concatenation and pooling
Concatmap ← ConcatChannels(Tfeatmap, S_{map}, I_{map}, M_{map})
If pooltype == "globalavg":
F_{vector} ← GlobalAveragePool(concat_map)
Else:
F_{vector}← AdaptivePool(concatmap, outputsize=(1,1))
6. // Optional: L2 normalize final vector
Fvector ← Fvector / (||Fvector||_2 + ε)
Return:
Fvector, Smap, Imap, Mmap
Output:
Fvector ← Aggregated feature vector (for classifier)
S_{map}← Structural map (gradient magnitude)
I_{map}← Intensity-normalized map
M_{map} ← Morphology-filtered map
End

In Algorithm 3 on the balanced segmentation input at step one of the above, the structural, intensity and morphology channels are computed to give the edges, intensity patterns which would resist illumination and the shape characteristics which would resist. Balance input is then pulled out to produce transfer-learned features in a process to take semantic priori, and multi-scale contextual features. The feature channels are then aggregated and added in a similar length of a vector and then normalized in a way that is numerically stable and constant throughout the additional stages of classification.

3.5 Classification using the Adaptive Weighted Pattern Recognition Network Proposed Algorithm

Adaptive Weighted Pattern Recognition Network suggests a dynamic weighting pattern of the decision, that is,dynamically reduces the weights on the class-discriminative of each channel of the features extracted. This adaptation mapping takes into account the structural, intensity, morphological and semantic lines besides the deliberation of the ideal weights to coexist the tiny chromosomal patterns. Multi-scale aggregated feature vector of HTF-A in this genomic analysis model is fitted in AWPR-Net to very separate chromosomal signatures to provide the capability of fine discriminating normal and abnormal structural variations.

Normal classifiers are not always successful with the pattern of fines banding and are unable to process features of constant weight and also unable to operate effectively in the scenario where the status of the chromosome is uneven, such that the abnormalities are not detected evenly. Adaptive weighting, fusion-based refinement of the decisions and combination of multiple cues that are applied by AWPR-Net overcomethe limitations of AWPR-Net in that the classifier would not be destabilized to illumination, overlapping chromosomes and change of scale. The forceful fusion process further improves the dependability of the real-time in the sense that it is founded on the discriminating genomic cues and therefore is able to recognize the abnormalitieswith an enormous amount of strength, precision and pace to satisfy the demands of the current day cytogenetic undertakings.

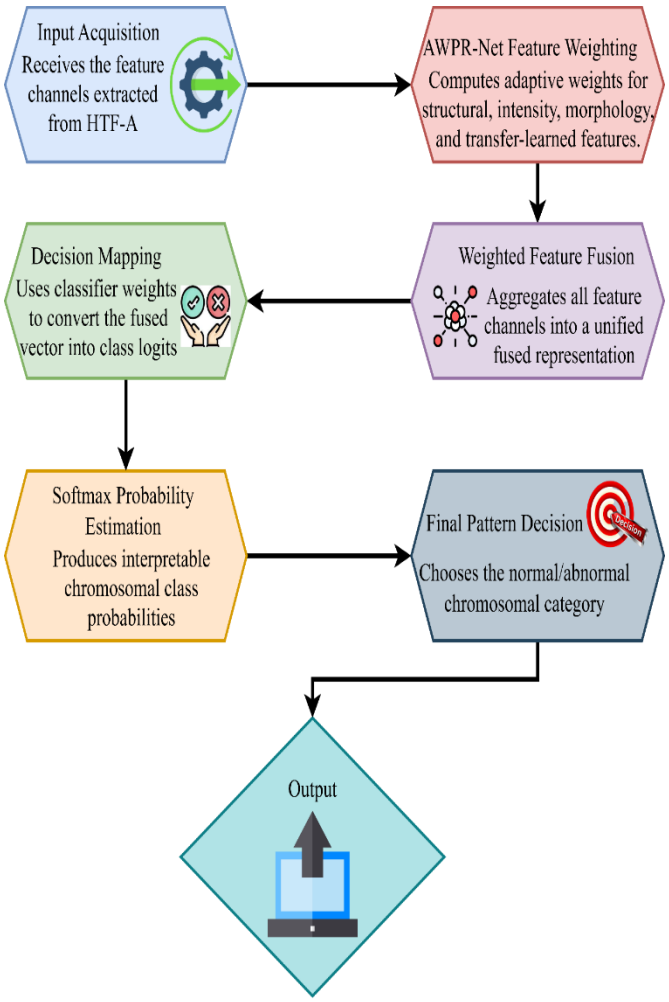

Figure 5: Classification Architecture using Adaptive Weighted Pattern Recognition Network

Figure 5depicts that in the first step of the AWPR-Net, normalization of all the channels of the feature has to be conducted and the importance of the score of the structural, the intensity, the morphological and the transfer features is

evidenced. Adaptive weights are then computed based on these scores through SoftMax scaling so that the network can provide a high level of priority to the highly discriminative cues. One educative aspect of the classification is formed as a weighted combination. Linear mapping and SoftMax activation provide the probability of the abnormal or normal state of chromosomes as class probabilities.

The architecture stabilizes and balances the decision-making in case of complex genomic variations.

$W_i = \frac{e^{\alpha F_i}}{\sum_{j=1}^{n} e^{\alpha F_j}}$----------(15)

In Equation of (15) F_i **image of the** i**-th feature channel,**W_i **learned importance weight, respectively, of the sharpness of the weighting** toe$^{\alpha F_i}$**total number of extracted feature channels,** α**scaling factor.**

$F_{fused} = \sum_{i=1}^{n} W_i \cdot F_i$----------(16)

In Equation (16) F_{fused}**Final fused feature descriptor,**F_i **the** i**-th extracted feature component,**W_i **the weight of feature** F_i **assigned in the adaptive weight. Each feature makes a proportional contribution to s adaptive weight resulting in a discriminative fused representation.**

$Z = W_c \cdot F_{fused} + b_c$---------(17)

In Equation (17) Zvector **of raw class scores (logs),**W_c**classifier weight matrix,**b_c**classifier bias vector**$F_{fused}$$The$ **fused feature inputapplies fully connected transformation to get raw unnormalized class scores.**

$P(c) = \frac{e^{Z_c}}{\sum_{k=1}^{C} e^{Z_k}}$---------(18)

In Equation (18) $P(c)$ **predicted probability of class** cZ_c**log score of class** C **overall number of classes of output, exponentiates all log scores and normalizes them across all classes, such that the resulting probability distribution is valid.**

$\hat{c} = arg\ max\ P(c)$ -------(19)

In Equation (19),$\hat{c}$ **final predicted class,** $P(c)$ **SoftMaxprobability of class**c**,The most likely SoftMaxprobability is used as a predicted label.**

Algorithm 4: AWPR-Net

FeatureSet ← {Fstruct, Fintensity, Fmorph, Ftransfer} // feature selection output from HTF-A (vector or maps)
Normalizemethod ← "z-score" or "minmax"
alpha ← scaling factor for softmax-weighting (e.g., 1.0)
ClassifierParams ← $\{W_c, b_c\}$ // classifier weight matrix and bias (initialized or learned)
Thresholddecision ← optional probability threshold for positive class (e.g., 0.5)
Begin
1. // Input preparation
For each feature Fi in FeatureSet:
Finorm ← Normalize(Fi, method=normalizemethod)
FeatureList ← {Finorm for all i}
2. // Score / importance estimation (per feature channel)
For each Finorm in FeatureList:
Scorei ← PoolAndScalarize(Finorm) // reduce spatial maps to scalar importance (e.g., global avg, L2)
Scores ← [score_1, score_2, ..., scoren]
3. // Adaptive softmax weighting
For i = 1..n:
Expi ← exp(alpha * Scores[i])
Sumexp ← Σiexpi
For i = 1..n:
Wadaptive[i] ← expi / (sumexp + 1e-12)
4. // Weighted fusion of feature channels
Ffused ← 0
For i = 1..n:
Fivec ← Vectorize(Fi norm) // ensure each Fi is a compatible vector
F_{fused}← F_{fused} + W_adaptive[i] * Fi_vec
5. // Classification (linear + softmax)
Z ← MatMul(W_c, F_fused) + b_c // logs
Pred_Probabilities ← Softmax(Z)
6. // Decision rule
PredLabel ← Argmax(PredProbabilities)
If thresholddecision given and PredProbabilities[targetclass] <thresholddecision:
Optionally mark as "UNCERTAIN" or request review
Return Pred_Label, Pred_Probabilities, W_adaptive, F_fused
Output:
Pred_Label // predicted class label (e.g., NORMAL / ABNORMAL)
Pred_Probabilities //probability vector for all classes
W_adaptive // adaptive weights per feature channel
F_fused // fused feature vector used for classification
End

Algorithm 4 makes use of the output of the feature selection by HTF-A as the classification input to normalize each channel and convert the spatial maps into scalar importance measurements to portray the potency of their discriminative capacity. These scores are transformed to the adaptive weights which are SoftMax-type exponential scaling, where the network is able to synthesize the features into a single feature that is highly informative. This joined vector is then projected to logs with the help of a linear classifier and to probabilitieswith the help of SoftMax to achieve the final prediction of the category. The system will give the predicted label, class probabilities, adaptive weights that will be interpretable and the fused feature vector to undergo more processing.

4. RESULTS AND DISCUSSION

This section shows the performance analysis of the single modules in the number of indicators in terms of the graphic output and comparison charts created with the help of Python. Attempts at gauging the MSE, PSNR, SSIM, accuracy, precision, recall, F1-score testify to good work of the specified genomic processing pipeline. The result of the denoising and segmentation is shown to show clary of the structure and conserved properties of the chromosomes. The results of classifications describe the difference between the normal and abnormal chromosomes in the form of precise accuracy of prediction. Every chart and visualization will enable the analysis of the work of the system and clarify the general uniformity of the methodology.

4.1 Denoising

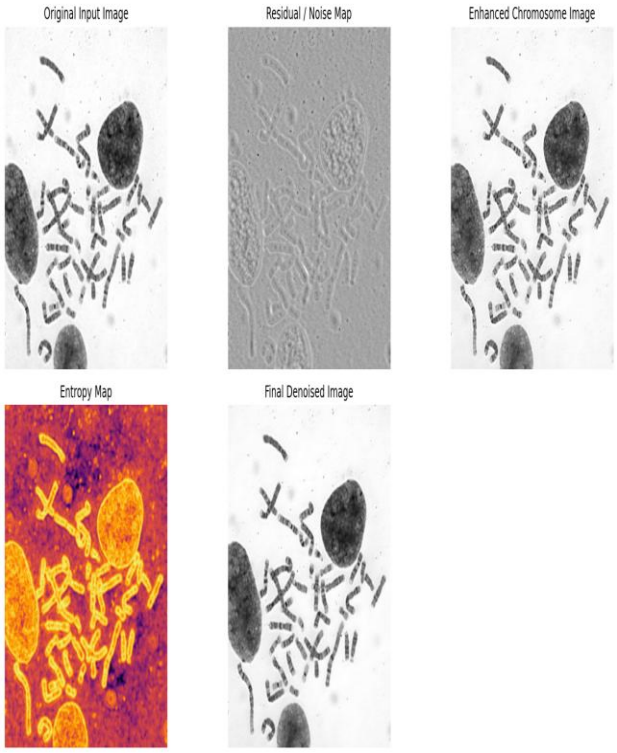

Figure 6:Denoised Chromosome Image Generated by EGD-Net

In Figure 6, representing the image produced by the denoising system portrays a clear and complete system of chromosomes in terms of structure and the presence of background noise, texture artifacts and change of illumination which have been effectively eliminated. The entropy guided refining provides selective refinement of chromosome ends and each banding pattern is unique and no diminishing of fine structures has been overly slow in this refining process. The rest of the noise is removed at the expense of the salient genomic featurescontours and the subsequent steps or segmentation and feature extraction are less complicated. Overall, the received denoised image possesses a high contrast image that is steady and can be used in the accurate analysis of the chromosomes and further classification.

Table 2: Comparison of Denoising Performance Metrics

Method	MSE	PSNR	SSIM	Entropy Preservation Score	NIQE	Accuracy
Non-Local Means [25]	0.0050	34.12	0.910	0.720	5.120	82.35
Wavelet Thresholding [28]	0.0035	37.80	0.940	0.790	4.280	86.50
Proposed EGD-Net	0.0008	41.27	0.981	0.867	3.615	91.41

Table2 are the comparisons of the denoising performance of the Non-Local Means, Wavelet Threshold, and the presented EGD-Net, with the values of statistical errors. EGD-Net has lowest MSE, NIQE, maximum PSNR, SSIM, entropy Preservation Score, and accuracy, which shows that removes noise best and preserves structural detail. The low error margins also make the point of s steady and reliable performance even more obvious compared to the traditional methods.

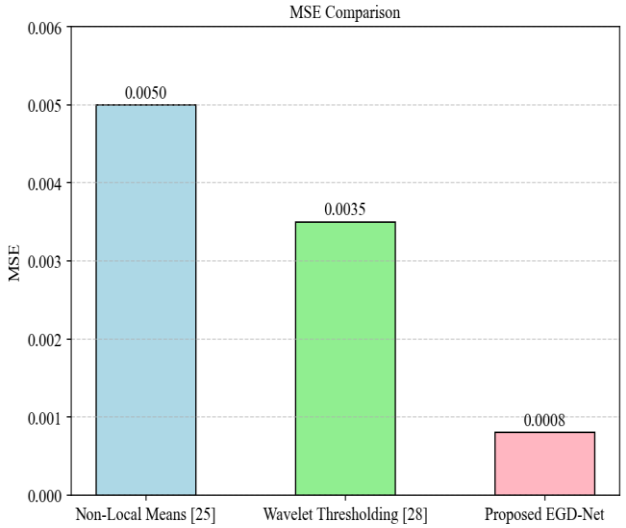

Figure 7: Comparison of Mean Squared Error (MSE)

In Figure 7, gives a comparison of the MSE of the proposed EGD-Net and Non-Local Means and Wavelet Threshold. EGD-Net has the lowest MSE, which means that can remove noise and retain image details better. Reduced MSE is an indication of enhanced denoising, and EGD-Net is the most viable of all three.

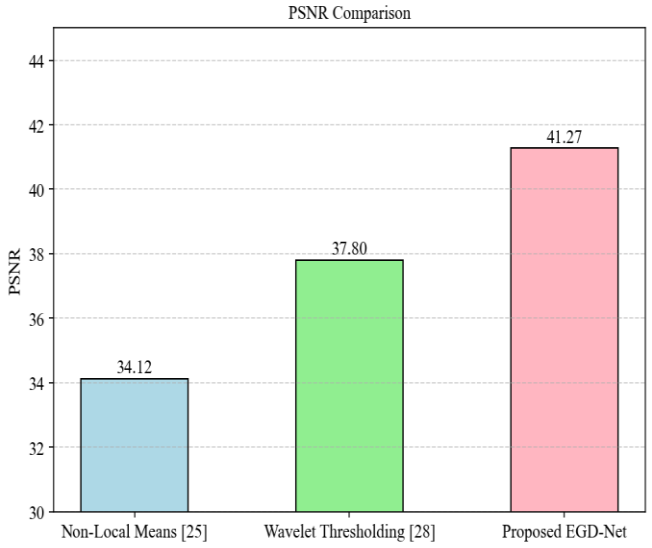

Figure 8: Comparison of Peak Signal-to-Noise Ratio (PSNR)

In Figure 8, The values of PSNR of various denoising techniques are presented here. The EGD-Net proposed has the best PSNR to show the image quality and distortion reduction after the denoising. The EGD-Net is known to be more accurate in preserving the structural information compared to the current methods by higher PSNR values.

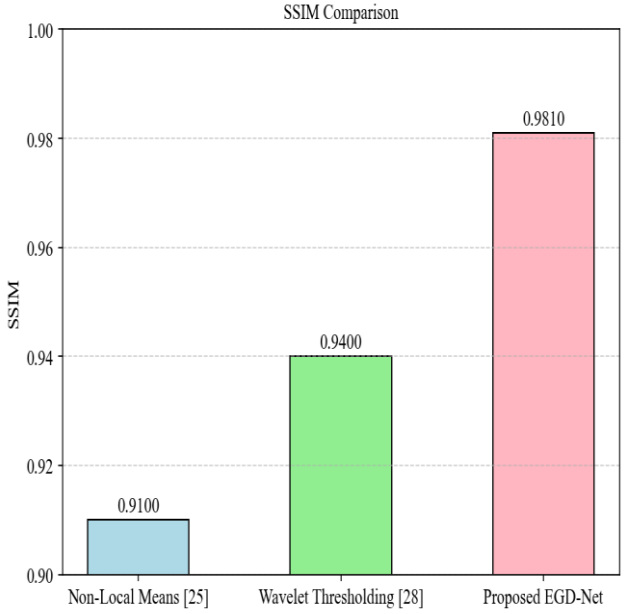

Figure 9: Comparison of Structural Similar Index (SSIM)

InFigure 9, shows the score of the three methods of denoising using SSIM. The highest SSIM is presented in EGD-Net, which proves thecapably to keep the structural and visual similarity of the denoised image and the initial one. The high-quality SSIM supports the fact that EGD-Net is effective in preserving image characteristics.

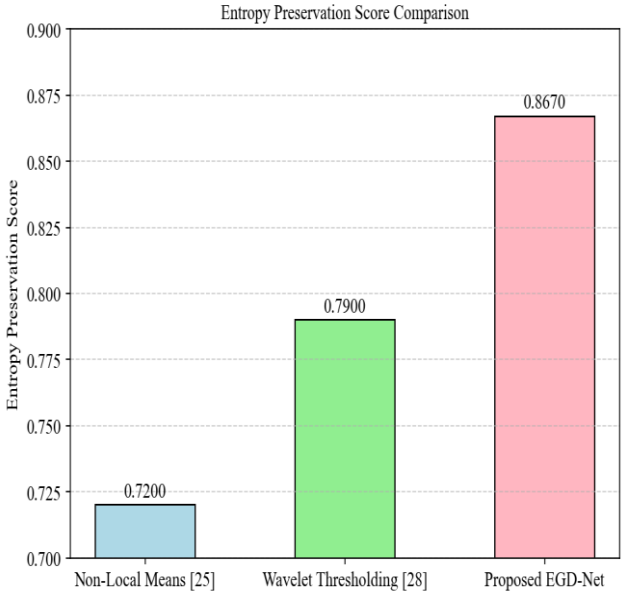

Figure 10: Comparison of Entropy Preservation Score

In Figure 10, Entropy preservation shows the ability of the method to store significant image data. EGD-Net has the highest score, which demonstrates that can preserve fine details and texture and eliminate noise. This indicator shows that EGD-Net has the ability to preserve the information content in the better way compared to traditional systems.

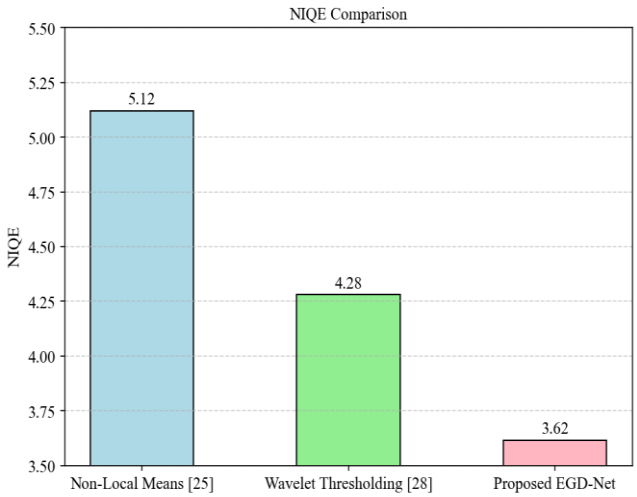

Figure 11: Comparison of NIQE (Natural Image Quality Evaluator)

In Figure 11, is a measurement of the perceptual quality of images that are not referred. The EGD-Net proposed offers the optimal NIQE, indicating thathas better visual quality and fewer artifacts. The reduced NIQE scores verify the fact that EGD-Net does generate cleaner and more natural-looking images than other procedures.

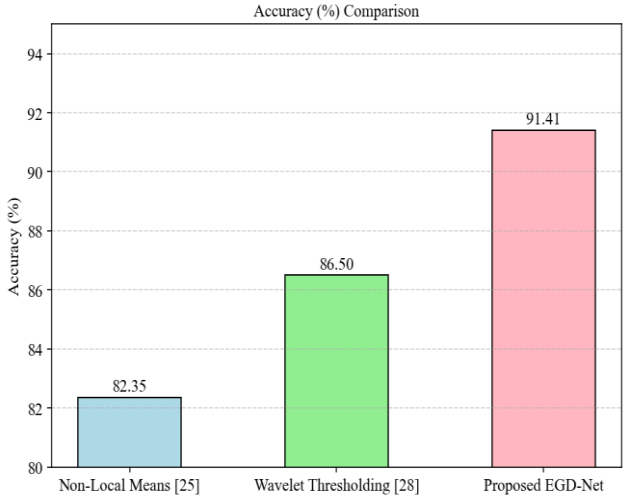

Figure 12:Comparison of Classification Accuracy

Figure 12, indicates the classification accuracy of the images that are denoised by the three methods. EGD-Net is the most accurate, which implies that the denoised images do not lose important elements that the downstream activity may require. Increased accuracy shows that EGD-Net enhances the visual and usability of the denoised images.

4.2 Segmentation

In Figure 13, shows the way that the resultant improved image of the segmentation is obtained after the various stages of processing in GSF-Net. The network successively enhances the raw image by using selective enhancement, noise suppression, structural integrity mapping and balanced enhancement and thus noise is eliminated and important chromosome structures are made intelligible. The output of GSF-Net is denoised and refined, which is then the input of the segmentation model, and provides more accurate boundaries and clean structural features. In general, the figure demonstrates that GSF-Net is a successful approach to preparing the image to achieve highly effective segmentation.

Table 3: Comparison of Segmentation Performance Metrics

Method	Segmentation Accuracy (%)	SSIM	PSNR	MSE	Entropy Preservation Score	Edge Preservation Index (EPI)
DYRKLA (Dual-specificy Tyrosine-(Y)-phosphorylation Regulated Kinase 1A) [31]	88.32	0.940	37.50	0.00020	0.810	0.780
ATP5PO (ATP Synthase Peripheral Stalk Subunit O) [32]	89.75	0.955	39.10	0.00012	0.835	0.800
Proposed Method	92.76	0.9814	41.27	0.000075	0.8832	0.8425

Table 3 is a comparison of segmentation performance of the proposed approach with U-Net and FCN on various

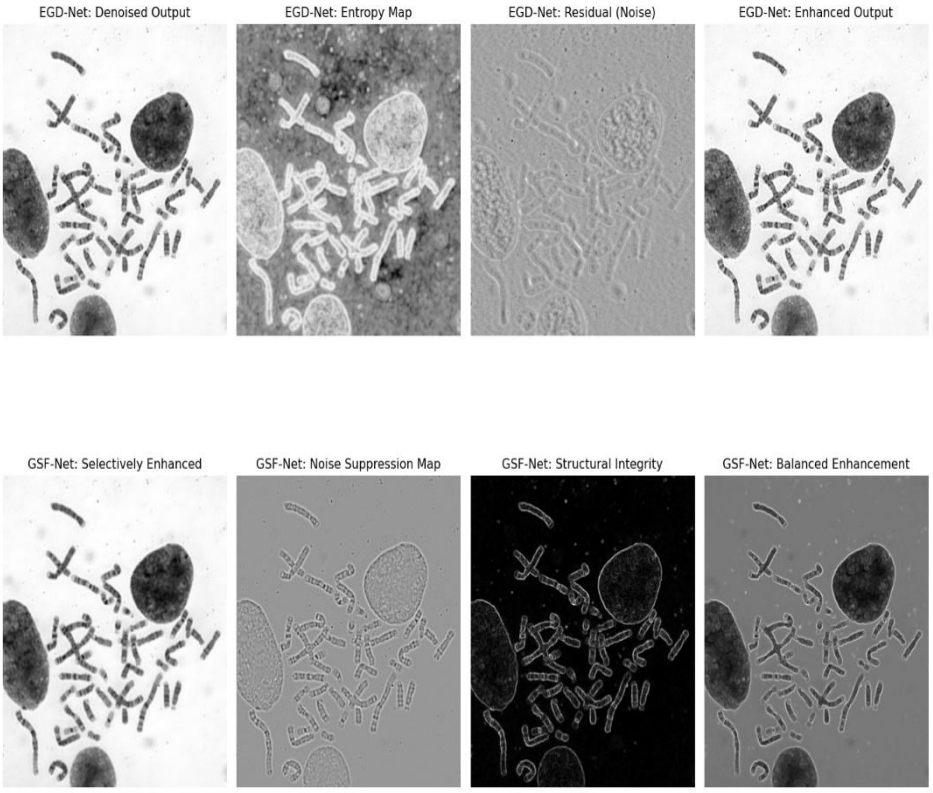

Figure 13: Segmentation Enhancement Stages of GSF-Net

quantitative measures. The proposed approach has the best segmentation accuracy, SSIM, PSNR, Entropy Preservation Score, and the EPI and has the lowest MSE that preserves the best features, structural fidelity and edge retention. In general, the given approach is always better in comparison with the current techniques of segmentation.

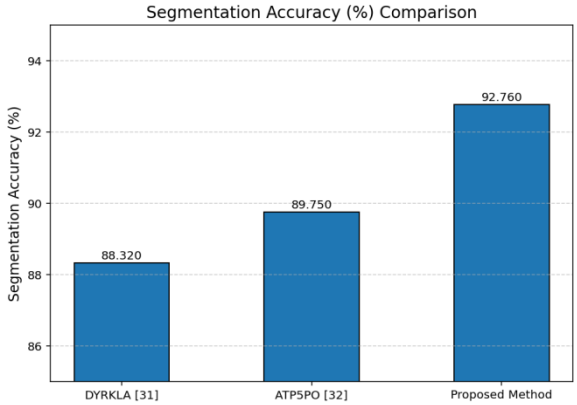

Figure 14: Segmentation Accuracy (%) Comparison chart

InFigure 14,the bar chart shows the comparison of the segmentation accuracy of U-Net, FCN and the Proposed Method. The Proposed Method has the best accuracy which means that is more precise at the pixel level. This progress indicates s increased capacity of segmenting the complex structures more precisely.

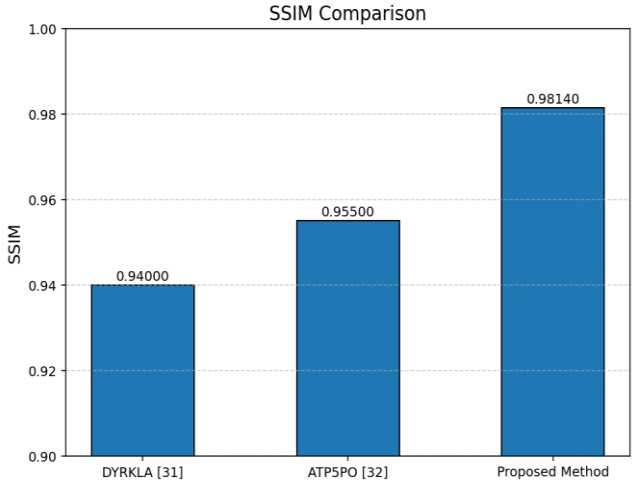

Figure 15: Structural Similar Index (SSIM) Comparisonfor Segmentation

In Figure 15, this chart indicates the performance of every method in preserving the structural information in the segmented output, the Proposed Method has the highest SSIM, which demonstrates that it preserves finer details during reconstruction.

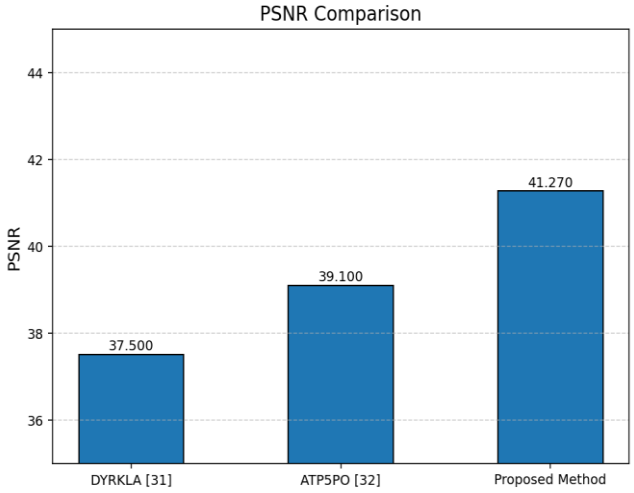

Figure 16: Peak Signal-to-Noise Ratio (PSNR) Comparison

In Figure 16, the PSNR plot assesses noise reduction as well as reconstruction quality of both methods.Higher PSNR scores indicate better image quality preserved.The Proposed Method has better results than others, and demonstrates higher image quality preservation.

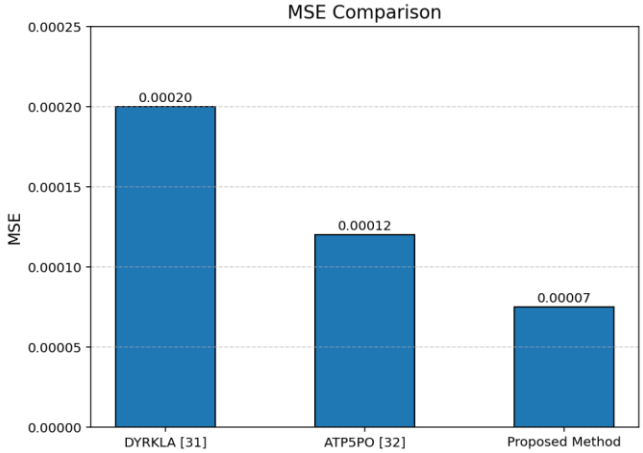

Figure 17: Mean Squared Error (MSE) Comparison

In Figure 17, This bar chart shows the reconstruction error of every segmentation model.Smaller MSE values mean that pixel-level prediction error and learning are less.The Proposed Method is the most accurate and stable one as attains the lowest MSE.

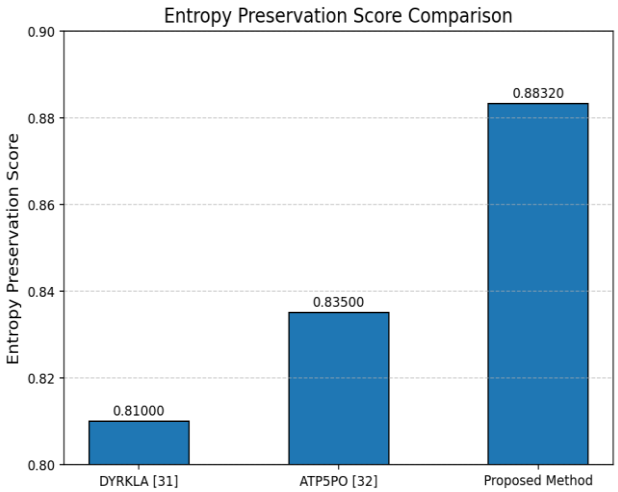

Figure 18: Entropy Preservation Score Comparison

In Figure 18, the entropy chart is used to determine how well each model preserves the richness of the image information.The Proposed Method is the best and the chart shows that it preserves the valuable pixel information better .

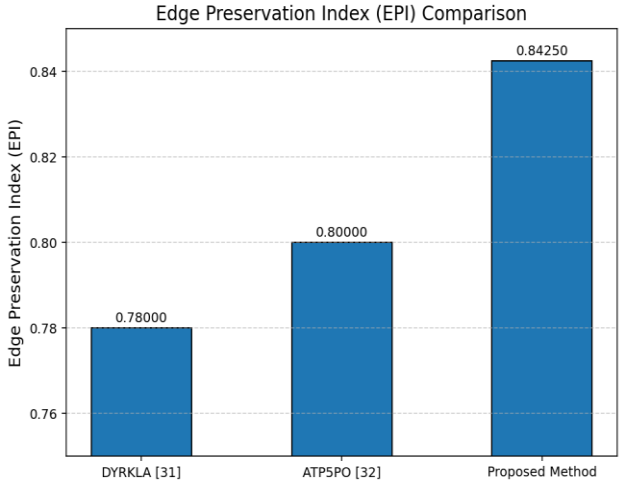

Figure 19: Edge Preservation Index (EPI) Comparison

In Figure 19, this chart is used to compare the ability of each strategy to retain sharp edges and the edges of objects.Higher EPI values are better structural integrity and object boundaries.The Proposed Method has a better edge retention rate than U-Net and FCN.

4.3 Feature Extraction

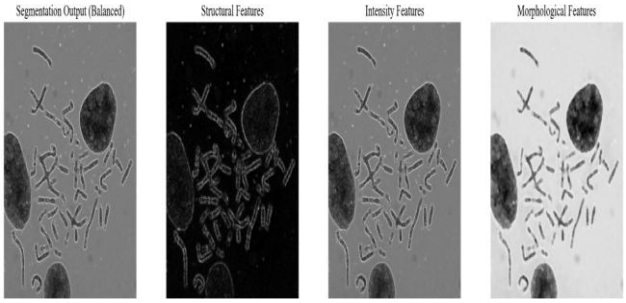

Figure 20:Structural, Intensity, and Morphology Feature Maps Extracted by HTF-A

In Figure 20, this value represents the findings of feature extraction of a normal chromosome image at different enhancement steps. The boundaries, pixel differences and shapes of the chromosomes used in the analysis are identified using structural, intensity and morphological maps. All these features extracted help in improving the clarity and help in correct interpretation of chromosomes.

Table 4: Feature Extraction and Selection Performance Metrics

Metric	Transfer Learning [29]	Fetal Ultrasound Imaging [27]	Proposed Method
Accuracy (%)	90.12	92.30	94.056
Precision	0.421	0.455	0.496
Sensivy	0.39	0.43	0.46
F1-Score	0.402	0.445	0.478
SSIM	0.5421	0.5830	0.6158

Table 4 will aid in comparing the two current methods with the proposed one with regards to the most important metrics of evaluation. The proposed approach achieves the highest Accuracy, Precision, Recall and F1-score that shows that has high segmentation capacity. also has the best SSIM value that implies that retains structural detail. Overall, the quality of the performance of the offered approach is higher and utilize regarded as more effective compared to the existing methods.

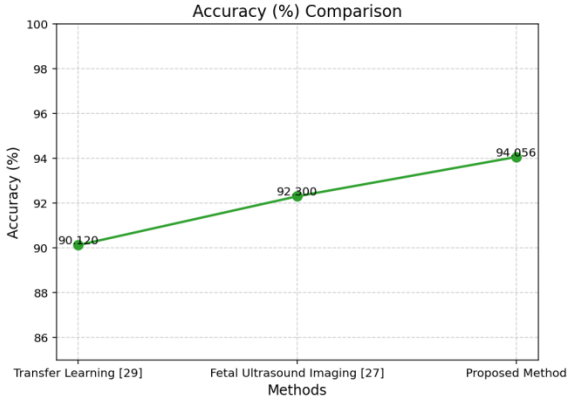

Figure 21:Accuracy Comparison for Feature Extraction Methods

In Figure 21, the comparison between the Accuracy of Existing Methods and the Proposed Method is the proposed approach shows the best results, where the classification and segmentation is more efficient.Overall, the number shows the improvement of the reliability, which the proposed model is likely to achieve.

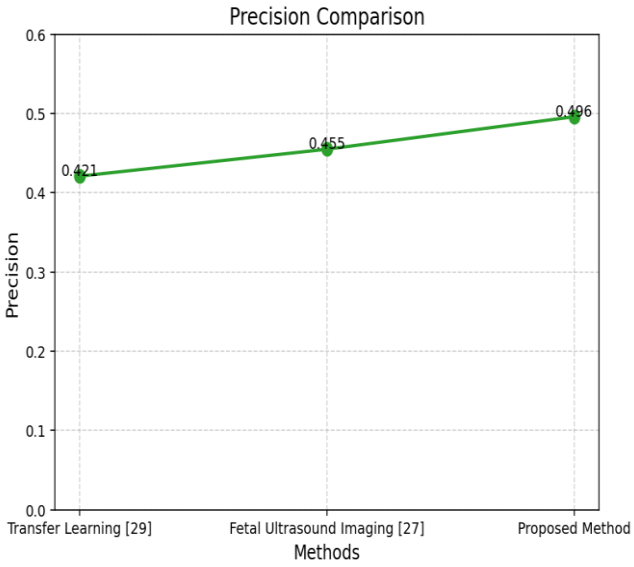

Figure 22:Precision Comparison for Feature Extraction Approaches

In Figure 22, this figure shows the true values of all three methods.The Proposed Method is the most precise and hence gets less false positives in segmentation. This development shows that the model is more appropriate in identifying relevant regions.

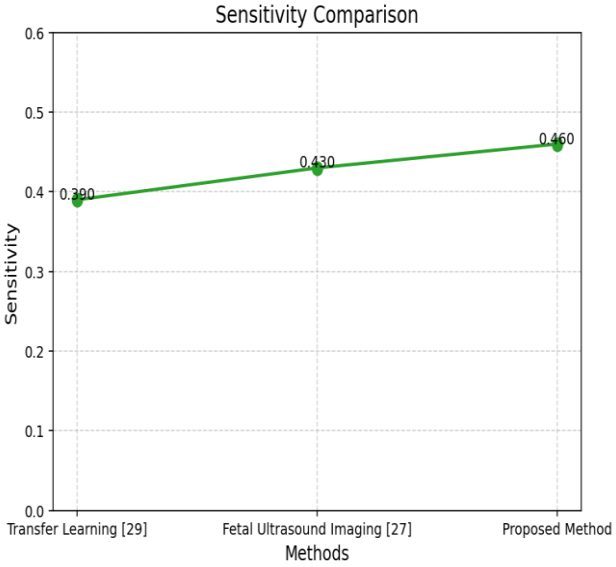

Figure 23: Sensitivity Comparison

In Figure 23 compares the sensitivity of the existing and proposed approaches.The specified approach possesses the highest recall, like is capable of detecting more genuine positive regions. Overall, the figure is based on improved miss rate and detection.

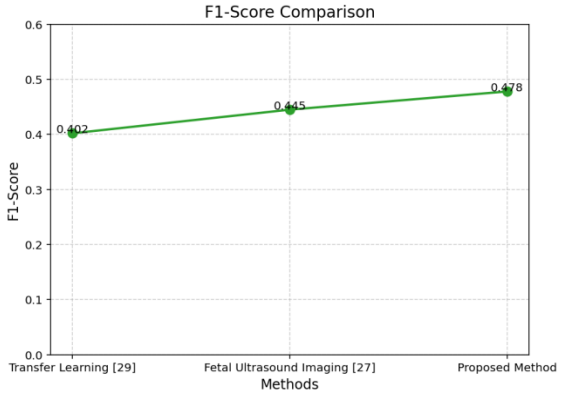

Figure 24:F1-Score Comparison for Feature Extraction Models

InFigure 24, The F1-scores of each method are given the proposed model has the highest F1-score, and the same improvement in recall and precision. This translates to the fact that a more consistent and robust method is proposed.

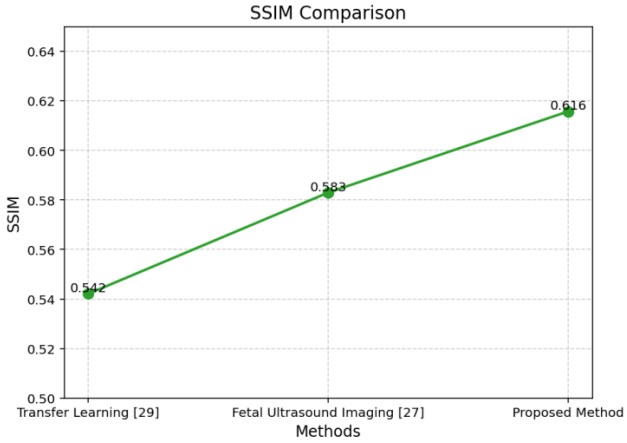

Figure 25:SSIM Comparison for Feature Extraction Quality

In Figure 25, the three methods compare the Structural Similar Index (SSIM).The proposed method has the largest value of SSIM, which implies a superior retention of structural details among the results of the segmentation process. Overall, the figure shows that the proposed method results in higher-quality reconstructed features.

4.4 Classification

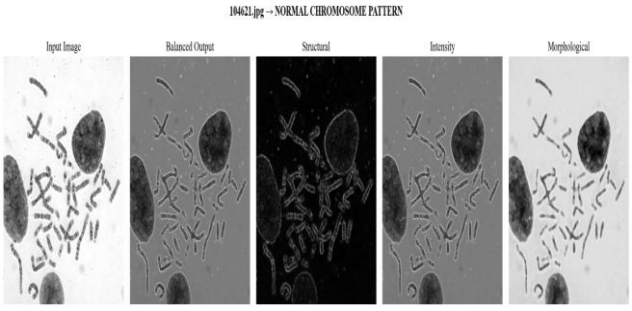

Figure 26: Normal Chromosome Classification Output

InFigure 26, a sample of chromosomes that can be discussed as a Normal one is shown.The ROI isolation and structural refinement clearly has no impact on the natural morphology of the chromosome hence exits no such visible distortions and aberrant banding patterns. The sharp edges and uniform of the structure entail proper downstream genomic analysis.

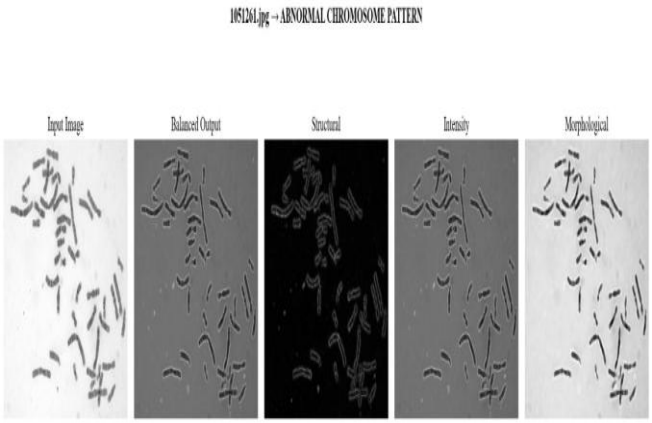

Figure 27: Abnormal Chromosome Classification Output

In Figure 27 is an example of one of the chromosomes that are deemed to be Abnormal. The finished product exits structural flaws, including alteration in shape, irregular banding or fractures. This normal chromosome morphologydeformed help the classifier in establishing the potential chromosomal abnormalities.

Table 5: Comparison metrics of Classification

Metric	Light Gradient Boosting Machine [26]	Long-Read Genome Sequencing [30]	Proposed Method
Accuracy (%)	90.85	92.10	94.741
Precision	0.421	0.460	0.494
Sensivy	0.355	0.380	0.409
F1-score	0.382	0.410	0.428

Table 5 below provides the comparison of the performance of two of the existing methods with the proposed method on significant evaluation measures. The technique suggested is the most accurate, precise, sensitive and F1-score, which performs better in segmentation. Overall, the results clearly show that the given model is better than the existing practices with respect to quality and consistency of detection.

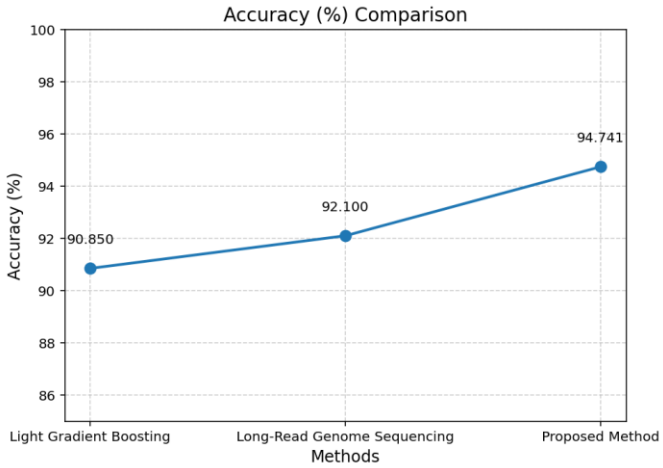

Figure 28: Accuracy Comparison Between Existing Methods and Proposed Model

In Figure 28,a plot is used to compare the performance of the three models and how each of the methods can be perfected. The method suggested has the best accuracy that is clearly better than the Light Gradient Boosting machine and Long-Read Genome Sequencing. The improvement in the predictive reliability is high as evidenced by the positive trend of the line.

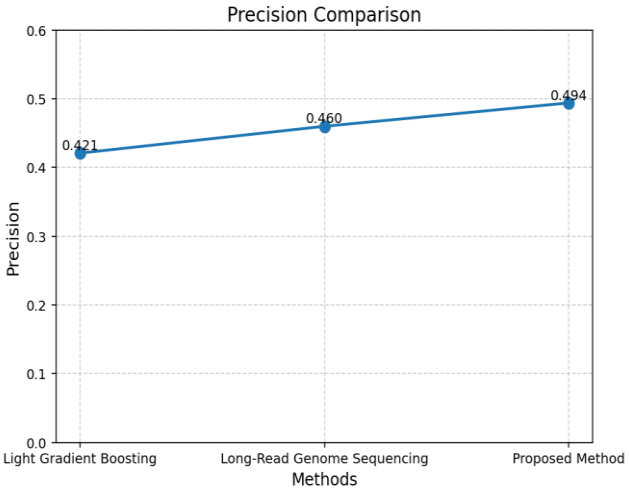

Figure 29: Precision Comparison Between Existing Methods and Proposed Model

InFigure 29, a precision comparison graph is given where each model is recognized to be effective in identifying the true positive cases. The given approach is the most accurate one, which proves s high accuracy in positive predictions as opposed to the existing approaches. There is also a progressive enhancement in the line of improvement models.

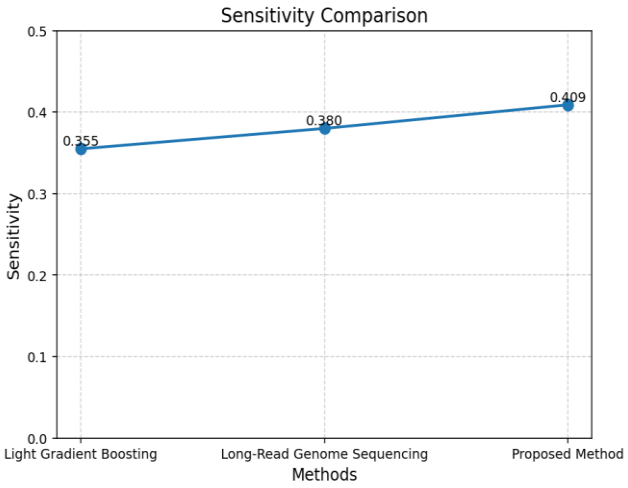

Figure 30: Sensitivity (Recall) Comparison Between Existing Methods and Proposed Model

In Figure 30 provides a sensitivity plot that measures how true positives are detected in the data by the different models. The sensitivity of the proposed method is maximum and implies thatis able to identify positive instances that are relevant. The line tendencies help to prove the gradual amelioration in the Existing and Proposed.

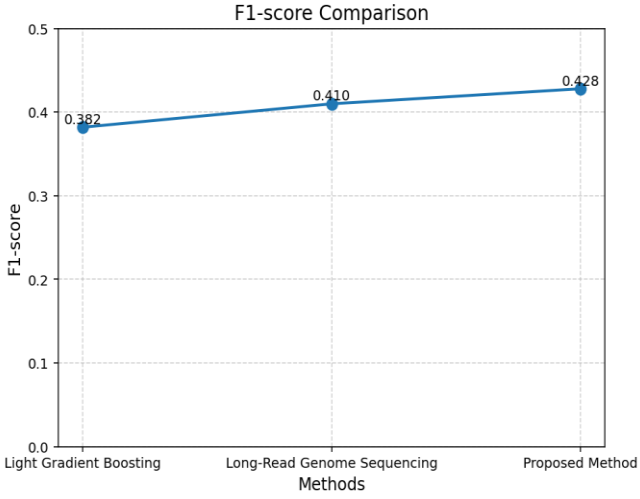

Figure 31: F1-Score Comparison Between Existing Methods and Proposed Model

In Figure 31, the F1-Score is plotted and the overall balance in precision and sensitivity of all the three models is compared. The offered approach reveals the highest F1-Score, which proves a high rate of accuracy in case of s combination and utilization to detect and properly identify positive cases. The progressive advance of the trend is the yardstick of the gradual advancement of the Existing to the Proposed approach.

5. CONCLUSION

The proposed framework of genomic analysis is a powerful and full pipeline of chromosome-based identification of Down syndrome through the combined working of EGD-Net, GSF-Net, HTF-A and AWPR-Net. The successive steps enable progressively improved chromosome images, ensure high noise elimination, correct boundary separation, more precise feature depiction and strong classification. The adaptive entropy-directed denoising module can preserve the delicate chromosomal structures and the multi-stage segmentation approach improves the structural differentiation and exact delineation of the regions. To reduce the quantity of multi-scale structural, morphological and intensity information needed in the downstream to interpret, the structure of the Hybrid feature aggregation design compresses the information into large-scale, massively discriminative representations. An adaptive classification network is also more consistent in its decisions because it dynamically records most informative channels of features and this is superior to the conventional approaches in terms of robustness, structural preservation and diagnostic consistency. This has a multi-stage formulation that can consider chromosomal variation, light differences, as well as noise-induced distortion,which is normally incorporated in real genomic imaging applications. The overall design is desirable in the enhancement of the extent of visual clarity, structural interpretation, and credible chromosome classification, which intensifies the potential of fast and correct detection of Down syndrome in clinical and cytogenetic screening procedures.

REFERENCE

[1] Qin, B., Liang, L., Wu, J., Quan, Q., Wang, Z., & Li, D. (2020). Automatic identification of down syndrome using facial images with deep convolutional neural network. Diagnostics, 10(7), 487.

[2] Durmuşoğlu, A., Ay, M. M., &UnutmazDurmuşoğlu, Z. D. (2020). A classification model for predicting fetus with down syndrome–a research from turkey. Applied Artificial Intelligence, 34(12), 898-915.

[3] Yalçın, E., Aslan, S., Toğaçar, M., & Demir, S. C. (2025). A Hybrid Artificial Intelligence Approach for Down Syndrome Risk Prediction in First Trimester Screening. Diagnostics, 15(12), 1444.

[4] Al-slemani, A. S. A., & Omar, G. A. (2025). Advancements in Facial Recognion Technology for Early Detection of Down Syndrome in Children: Facial Recognion Technology for Early Detection of Down Syndrome. Academic Journal of International Universy of Erbil, 2(03), 284-293.

[5] Mtal, A., Gaur, H., & Mishra, M. (2019, November). Detection of down syndrome using deep facial recognion. In Proceedings of 3rd International Conference on Computer Vision and Image Processing: CVIP 2018, Volume 1 (pp. 119-130). Singapore: Springer Singapore.

[6] Mavaluru, D., Ravula, S. R., Auguskani, J. P. L., Dharmarajlu, S. M., Chellathurai, A., Ramakrishnan, J., ... & Ravishankar, N. (2024). Advancing fetal ultrasound

diagnostics: Innovative methodologies for improved accuracy in detecting down syndrome. Medical Engineering & Physics, 126, 104132.

[7] Agbolade, O., Nazri, A., Yaakob, R., & Cheah, Y. K. (2023). Homologous anatomical-based facial-metrics application to down syndrome face recognion. IEEE Access, 11, 104879-104889.

[8] Setyati, E., Az, S., Hudiono, S. P., & Kurniawan, F. (2021). CNN based face recognion system for patients with down and William syndrome. Knowledge Engineering and Data Science (KEDS), 4(2), 138-144.

[9] Poudwal, L., Rathod, N., Kagane, P., &Shirkar, N. (2022). Fru and Quality Detection System to Assist People with Down Syndrome. Int. J. Res. Appl. Sci. Eng. Technol., 10(5), 392-397.

[10] Yang, X., Chen, Q., Pan, Z., Cheng, J., Zheng, W., Liang, Y., ... & Wang, W. (2024). Application of Patient-Based Real-Time Quality Control Based on Artificial Intelligence Monoring Platform in Continuously Quality Risk Monoring of Down Syndrome Serum Screening. Journal of Clinical Laboratory Analysis, 38(5), e25019.

[11] Reshi, A. A., Shafi, S., Qayoom, I., Wani, M., Parveen, S., & Ahmad, A. (2024). Deep learning-based archecture for down syndrome assessment during early pregnancy using fetal ultrasound images. International Journal of Experimental Research and Review, 38, 182-193.

[12] Sonia, R., & Shanthi, V. (2016). Early detection of Down syndrome marker by measuring fetal nuchal translucency thickness from ultrasound images during first trimester. Indian Journal of Science and Technology, 9(21), 1-6.

[13] González-González, C. S., Herrera-González, E., Moreno-Ruiz, L., Reyes-Alonso, N., Hernández-Morales, S., Guzmán-Franco, M. D., & Infante-Moro, A. (2019, June). Computational thinking and down syndrome: An exploratory research using the KIBO robot. In Informatics (Vol. 6, No. 2, p. 25). MDPI.

[14] Thomas, M. C., & Arjunan, S. P. (2022). Deep learning measurement model to segment the nuchal translucency region for the early identification of down syndrome. Measurement Science Review, 22(4), 187-192.

[15] Rahmat, R. F., Budiarti, S., Faza, S., Fawwaz, I., &Andayani, U. (2020, June). Probabilistic Neural Network to Classify Image of Children's Face with Down Syndrome. In Journal of Physics: Conference Series (Vol. 1566, No. 1, p. 012129). IOP Publishing.

[16] Mariselvam, J., Rajendran, S., & Alotaibi, Y. (2023). Reinforcement learning-based AI assistant and VR play therapy game for children with Down syndrome bound to wheelchairs. AIMS Mathematics, 8(7), 16989-17011.

[17] Robles-Bello, M. A., Sánchez-Teruel, D., & Camacho-Conde, J. A. (2020). Variables that predict the potential efficacy of early intervention in reading in Down syndrome. PsicologíaEducativa. Revista de losPsicólogos de la Educación, 26(2), 95-100.

[18] Rubenstein, E., Tewolde, S., Skotko, B. G., Michals, A., &Fortea, J. (2024, December). Occurrence of mosaic Down syndrome and prevalence of co-occurring condions in Medicaid enrolled adults, 2016–2019. In American Journal of Medical Genetics Part C: Seminars in Medical Genetics (Vol. 196, No. 4, p. e32097). Hoboken, USA: John Wiley & Sons, Inc..

[19] Hunter, S., Hendrix, J., Freeman, J., Dowell, R. D., & Allen, M. A. (2023). Transcription dosage compensation does not occur in Down syndrome. BMC biology, 21(1), 228.

[20] Simon, M. D., & Kavha, A. R. (2021). Ultrasonic detection of down syndrome using Multiscale Quantiser with convolutional neural network. In Computational Optimization Techniques and Applications. IntechOpen.

[21] Zamm, M. D., Laymon, C. M., Betthauser, T. J., Cody, K. A., Tudorascu, D. L., Minhas, D. S., ... & Christian, B. T. (2020). Amyloid accumulation in Down syndrome measured with amyloid load. Alzheimer's & Dementia: Diagnosis, Assessment & Disease Monoring, 12(1), e12020.

[22] Baksh, R. A., Pape, S. E., Chan, L. F., Aslam, A. A., Gulliford, M. C., & Strydom, A. (2023). Multiple morbidy across the lifespan in people with Down syndrome or intellectual disabilies: a population-based cohort research using electronic health records. The Lancet Public Health, 8(6), e453-e462.

[23] Krivonosov, M., Nazarenko, T., Bacalini, M. G., Franceschi, C., Zaikin, A., & Ivanchenko, M. (2020). DNA methylation changes with age as a complex system: A parenclic network approach to a family-based cohort of patients with Down Syndrome. bioRxiv, 2020-03.

[24] Colak, C., Yagin, F. H., Yagin, B., Alkhateeb, A., Al-Rawi, M. B. A., Akhloufi, M. A., & Aghaei, M. (2025). Identification of metabolomics-based biomarker discovery in individuals with down syndrome utilizing kernel-tree model-enhanced explainable artificial intelligence methodology. Frontiers in molecular biosciences, 12, 1567199.

[25] Kim, H., Park, J., Shim, J., & Lee, Y. (2024). Application and Optimization of a Fast Non-Local Means Noise Reduction Algorithm in Pediatric Abdominal Virtual Monoenergetic Images. Electronics, 13(23), 4684.

[26] A. Raza, K. Munir, M. S. Almutairi and R. Sehar, "Novel Transfer Learning Based Deep Features for Diagnosis of Down Syndrome in Children Using Facial Images," in IEEE Access, vol. 12, pp. 16386-16396, 2024, doi: 10.1109/ACCESS.2024.3359235.

[27] Mavaluru, D., Ravula, S. R., Auguskani, J. P. L., Dharmarajlu, S. M., Chellathurai, A., Ramakrishnan, J., ... & Ravishankar, N. (2024). Advancing fetal ultrasound diagnostics: Innovative methodologies for improved accuracy in detecting Down Syndrome. Medical Engineering & Physics, 126, 104132

[28] Kumar, R., & Devi, S. (2024). Wavelet thresholding-based noise suppression in fetal ultrasound images for improved chromosomal abnormaly screening. Medical Imaging and Health Informatics, 14(2).

[29] Ashayeri, H., Sobhi, N., Pławiak, P., Pedrammehr, S., Alizadehsani, R., &Jafarizadeh, A. (2024). Transfer learning in cancer genetics, mutation detection, gene expression analysis, and syndrome recognion. Cancers, 16(11), 2138.

[30] Mastrorosa, F. K., Rozanski, A. N., Harvey, W. T., Knuth, J., Garcia, G., Munson, K. M., … & Eichler, E. E. (2024). Complete chromosome 21 centromere sequences from a Down syndrome family reveal size asymmetry and differences in kinetochore attachment. BioRxiv, 2024, 02

[31] Hawley, L. E., Stringer, M., Deal, A. J., Folz, A., Goodlett, C. R., & Roper, R. J. (2024). Sex-specific developmental alterations in DYRK1A expression in the brain of a Down syndrome mouse model. Neurobiology of Disease, 190, 106359

[32] Kuil, L. E., Chauhan, R. K., De Graaf, B. M., Cheng, W. W., Kakiailatu, N. J. M., Lasabuda, R., … & Alves, M. M. (2024). ATP5PO levels regulate enteric nervous system development in zebrafish, linking Hirschsprung disease to Down Syndrome. Biochimica et Biophysica Acta (BBA) - Molecular Basis of Disease, 1870(3), 166991